Multiphoton above-threshold detachment of Li^-: Exterior-complex-scaling–generalized-pseudospectral method for calculations of complex-quasienergy resonances in Floquet formulation of time-dependent density-functional theory

Dmitry A. Telnov* and Shih-I Chu
Department of Chemistry, University of Kansas, Lawrence, Kansas 66045
and Kansas Center for Advanced Scientific Computing, Lawrence, Kansas 66045
(Received 22 February 2002; published 25 October 2002)

We extend the exterior-complex-scaling–generalized-pseudospectral (ECSGPS) method [D. A. Telnov and S. I. Chu, Phys. Rev. A **59**, 2864 (1999)] to the nonperturbative calculations of complex-quasienergy resonances of many-electron quantum systems within the Floquet formulation of time-dependent density-functional theory (TDDFT) [D. A. Telnov and S. I. Chu, Chem. Phys. Lett. **264**, 466 (1997)]. The ECSGPS technique appears very useful in TDDFT-Floquet calculations where the exchange-correlation potentials may exhibit quite complicated behavior as functions of the electron coordinates and cannot be easily treated by means of the uniform-complex-scaling techniques. We have applied this procedure to the study of one-photon detachment and two-photon dominant above-threshold detachment of Li^- negative ions. In the one-photon case, the photodetachment cross section has been calculated as a function of the photon energy with results in good agreement with the experimental data. In the two-photon case, both the partial detachment rates and electron angular distributions for the dominant and above-threshold channels are presented for a range of laser field frequencies and intensities. Dramatic transformations of the angular distributions in the vicinity of the two-photon threshold are observed and analyzed.

DOI: 10.1103/PhysRevA.66.043417 PACS number(s): 32.80.Rm, 32.80.Gc, 31.15.Ew

I. INTRODUCTION

Density-functional theory (DFT) for stationary properties of many-electron systems, based on the earlier fundamental works of Hohenberg and Kohn [1] and Kohn and Sham [2], is now a well established and is a practical tool in various branches of chemistry and physics [3]. It is a formalism of many-body theory in terms of the electron density $\rho(\boldsymbol{r})$. DFT proves to be accurate and computationally much less expensive than the *ab initio* wave-functional methods and this accounts for its great success in the time-independent electron-structure calculations of the ground states of many-electron systems.

To study the more interesting dynamical processes, one needs the time-dependent DFT (TDDFT) [4–7]. The central theme of TDDFT is a set of time-dependent Kohn-Sham (TDKS)-like equations that are structurally similar to the time-dependent Hartree-Fock equations but include, in principle, exactly all many-body effects, through a local time-dependent exchange-correlation (xc) potential. Most of the applications of TDDFT before mid-1990s fall in the regime of linear or nonlinear response in weak fields for which the perturbation theory is applicable [4–10]. More recently, the TDDFT has been generalized to the intense field regime for the study of multiphoton processes of atomic [11–14] and molecular [15,16] systems. One of the major efforts is to develop procedures for removing the self-interaction energy contained in the explicit xc energy functionals in the time domain [11–16]. Another major effort is to develop more efficient and accurate numerical procedures such as the time-dependent generalized-pseudospectral methods [12,14–16] for the solution of self-interaction-free TDDFT equations.

Recently, an alternative nonperturbative and time-independent formulation of the TDDFT and time-dependent current DFT [17], based on the extension of the generalized Floquet formalism [18], was developed, allowing exact transformation of the TDKS-like equations into an equivalent time-independent non-Hermitian Floquet matrix eigenvalue problem [19–22]. Such a TDDFT-Floquet formalism provides a general time-independent approach for nonperturbative treatment of multiphoton processes of many-electron quantum systems in periodic, quasiperiodic, or multicolor laser fields.

The motivations of this paper are twofold. First, we apply the TDDFT-Floquet formalism introduced in our previous studies [19–22] to multiphoton and above-threshold detachment of Li^- negative ion. Second, we extend our recent exterior-complex-scaling–generalized-pseudospectral technique (ECSGPS) [23] to TDDFT-Floquet formulation. The ECSGPS method allows for accurate and efficient treatment of resonance states such as complex-quasienergy resonances associated with multiphoton above-threshold detachment of Li^-. The ECSGPS technique not only provides a simplified procedure for the calculation of partial rates and electron angular distributions [23], as compared with the uniform-complex-scaling methods, but also allows treatment of complicated potentials with singularities in the complex coordinate plane, which may cause problems when used in the uniform-complex-scaling procedures. The latter circum-

*Permanent address: Institute of Physics, St. Petersburg State University, 198904 St. Petersburg, Russia. Electronic address: telnov@pcqnt1.phys.spbu.ru

stance is especially important for DFT and TDDFT applications where the modern exchange-correlation potentials have quite sophisticated expressions.

The paper is organized as follows. In Sec. II, we outline the basic equations of the Floquet formulation of TDDFT. Section III briefly describes the ECSGPS technique. In Sec. IV, we apply Floquet formulation of TDDFT and ECSGPS procedure to the study of multiphoton above-threshold detachment of Li^-.

II. NON-HERMITIAN FLOQUET FORMULATION OF TIME-DEPENDENT DENSITY-FUNCTIONAL THEORY

Recently, we developed the Floquet formulation of time-dependent density-functional and current density-functional theories [19–22]. The TDDFT-Floquet theory can be applied to the nonperturbative study of multiphoton processes of many-electron atoms and molecules in intense periodic or quasiperiodic (multicolor) time-dependent fields, allowing the reduction of time-dependent Kohn-Sham equations to equivalent *time-independent* Floquet matrix eigenvalue problems.

Consider the time-dependent Schrödinger equation (atomic units are used throughout the paper)

$$i\frac{\partial}{\partial t}\Psi(\boldsymbol{R},t)=\hat{H}(t)\Psi(\boldsymbol{R},t). \tag{1}$$

Here $\Psi(\boldsymbol{R},t)$ is a wave function of a *many-electron* system (notation $\boldsymbol{R}$ stands for all coordinates of the system under consideration). We assume the Hamiltonian $\hat{H}(t)$ is periodic in time:

$$\hat{H}(t+T)=\hat{H}(t) \tag{2}$$

(T is the period; one can introduce also the fundamental frequency ω defined as $\omega=2\pi/T$). The Floquet theorem (see Refs. [18,24,25]) allows one to search for a solution of Eq. (1) in the following form:

$$\Psi(\boldsymbol{R},t)=\exp(-i\varepsilon t)\Phi(\boldsymbol{R},t), \tag{3}$$

where ε is the *quasienergy* and $\Phi(\boldsymbol{R},t)$ is a periodic function of time, $\Phi(\boldsymbol{R},t)=\Phi(\boldsymbol{R},t+T)$. Equation (1) can be recast in the form of the quasienergy eigenvalue equation [18,24,25]:

$$\hat{\mathcal{H}}\Phi(\boldsymbol{R},t)=\varepsilon\Phi(\boldsymbol{R},t), \tag{4}$$

$$\hat{\mathcal{H}}=\hat{H}(t)-i\frac{\partial}{\partial t}. \tag{5}$$

Consider the *extended* Hilbert space $\mathcal{S}$ containing all square-integrable time-periodic functions $\Phi(\boldsymbol{R},t)$ [18,25]. The inner product in this space is defined as

$$\langle\langle\Phi|\Xi\rangle\rangle=\frac{1}{T}\int_0^T dt\langle\Phi|\Xi\rangle. \tag{6}$$

The operator $\hat{\mathcal{H}}$ defined in Eq. (5) is a self-adjoint operator in the Hilbert space $\mathcal{S}$. Its eigenstates that are the solutions of Eq. (4) constitute a complete set in $\mathcal{S}$. Note that the following transformation:

$$\varepsilon'=\varepsilon+m\omega, \tag{7}$$

$$\Phi'(\boldsymbol{R},t)=\exp(im\omega t)\Phi(\boldsymbol{R},t), \tag{8}$$

where m is an arbitrary integer number, converts any eigenstate in Eq. (4) into another eigenstate. Thus for any Floquet state $\Phi(\boldsymbol{R},t)$ there is an infinite set of other Floquet states, and the quasienergies for those states differ by an integer number of ω.

In the Floquet formulation of TDDFT, the main role is played by the *quasienergy functional* (compare with the *action functional* in the general time-dependent formulation [7]):

$$F[\Phi]=\langle\langle\Phi|\hat{\mathcal{H}}|\Phi\rangle\rangle. \tag{9}$$

The variation of the functional (9) under the normalization condition

$$\langle\langle\Phi|\Phi\rangle\rangle=1 \tag{10}$$

leads to the Eq. (4) for the time-periodic multielectron wave function $\Phi(\boldsymbol{r},t)$. The solution brings the stationary value (equal to the quasienergy ε) to the functional (9).

For the time-dependent Schrödinger equation (1), one normally has an initial-state problem: once the initial state is specified at $t=t_0$, then the solution of the time-dependent Schrödinger equation is unique and the wave function can be constructed at any time t. It is well known that the action functional in TDDFT [7] is a unique functional of the density provided the *initial state* is fixed. For the Floquet states, however, one does not have an initial-state problem. Instead, one has an *eigenvalue* problem in the extended Hilbert space $\mathcal{S}$. That means, instead of specifying the initial state, one imposes the *boundary* conditions on the solution of the equation, so there is no concept of the initial state for the eigenvalue problem. Accordingly, there is no concept of the initial state in the Floquet formulation of TDDFT. The Floquet states are the *eigenstates* of the Hermitian operator $\hat{\mathcal{H}}$ in the extended Hilbert space $\mathcal{S}$. In this respect, Floquet formulation of TDDFT resembles the time-independent DFT. The quasienergy functional in the Floquet formulation of TDDFT depends on the particular Floquet state, like it holds in the time-independent DFT: the traditional time-independent DFT based on the Hohenberg-Kohn theorem is applicable to the *ground* states only. However, unlike the time-independent atomic and molecular Hamiltonians, the Floquet Hamiltonian does not possess a ground state: for any quasienergy ε there is also an infinite set of quasienergies $\varepsilon+m\omega$, m being an arbitrary integer number [Eqs. (7) and (8)]. Nevertheless, the time-independent DFT can be reformulated in the way that all the eigenstates (not just the ground state) are treated on the same footing [26]. That provides a rigorous basis for treatment of the excited states by density-functional methods. The dependence on the particular eigenstate still re-

mains in the theory [26] since the density functionals are different for different eigenstates. We apply the Floquet formulation of TDDFT to the Floquet states that originate from the field-free *ground* states of atomic (molecular) systems upon adiabatic switch on the external time-periodic field. With this choice of the state, the quasienergy functional (9) becomes a unique functional of the electron density (spin densities in the spin-polarized case).

Consider the corresponding Kohn-Sham system of noninteracting particles with the same electron spin densities. As the spin densities are periodic in time, the quasienergy solutions of the corresponding time-dependent Schrödinger equations may be sought, and one can introduce the time-periodic Kohn-Sham spin orbitals $\phi_k^\sigma(\boldsymbol{r},t)$ (the superscript σ stands for the spin projection, it can take values α and β for the spin-up and spin-down, respectively; the subscript k enumerates the orbitals with the same spin). Denoting ρ^σ as the spin density corresponding to the spin σ, and ρ is the total density:

$$\rho^\sigma(\boldsymbol{r},t)=\sum_k |\phi_k^\sigma(\boldsymbol{r},t)|^2, \tag{11}$$

$$\rho(\boldsymbol{r},t)=\sum_\sigma \rho^\sigma(\boldsymbol{r},t), \tag{12}$$

one can rewrite the quasienergy functional (9) in the following form [22]:

$$F[\rho^\alpha,\rho^\beta]=\frac{1}{T}\int_0^T dt\ [T_s(t)+J(t)+U(t) + V_{ext}(t)+D_s(t)+E_{xc}(t)]. \tag{13}$$

The time-dependent quantities under the integral (13) are defined as follows:

$$T_s(t)=\sum_{k,\sigma}\left\langle \phi_k^\sigma(\boldsymbol{r},t)\ \middle|\ -\frac{1}{2}\nabla^2\ \middle|\ \phi_k^\sigma(\boldsymbol{r},t)\right\rangle, \tag{14}$$

$$J(t)=\frac{1}{2}\int d^3r\int d^3r'\ \frac{\rho(\boldsymbol{r},t)\rho(\boldsymbol{r}',t)}{|\boldsymbol{r}-\boldsymbol{r}'|}, \tag{15}$$

$$U(t)=\int d^3r\rho(\boldsymbol{r},t)u(\boldsymbol{r}), \tag{16}$$

$$V_{ext}(t)=\int d^3r\rho(\boldsymbol{r},t)v_{ext}(\boldsymbol{r},t), \tag{17}$$

$$D_s(t)=\sum_{k,\sigma}\left\langle \phi_k^\sigma(\boldsymbol{r},t)\ \middle|\ -i\frac{\partial}{\partial t}\ \middle|\ \phi_k^\sigma(\boldsymbol{r},t)\right\rangle. \tag{18}$$

Here $T_s(t)$ is a noninteracting kinetic energy, $J(t)$ is a classical electron-electron repulsion (Hartree) energy, $U(t)$ is an expectation value of a single-particle potential (interaction with the nucleus), $V_{ext}(t)$ is an expectation value of the external field, and $E_{xc}(t)$ is the exchange-correlation energy. The latter is an unknown functional of the time-dependent spin densities. The simplest approximation for this functional is the adiabatic local-density approximation (ALDA) [4], straightforward extension of steady-state LDA to the time-dependent domain, preserving locality in both coordinate space and time.

The quasienergy Kohn-Sham equations for the time-periodic spin orbitals ϕ_k^σ are obtained from the stationary principle for the quasienergy functional (13):

$$\left[-\frac{1}{2}\nabla^2+u(\boldsymbol{r})+v_H(\boldsymbol{r},t)+v_{xc}(\boldsymbol{r},t) + v_{ext}(\boldsymbol{r},t)-i\frac{\partial}{\partial t}\right]\phi_k^\sigma=\epsilon_k^\sigma\phi_k^\sigma. \tag{19}$$

Here $v_H(\boldsymbol{r},t)$ is the Hartree potential, $v_{xc}(\boldsymbol{r},t)$ is the exchange-correlation potential, $v_{ext}(\boldsymbol{r},t)$ is the external field potential, and ϵ_k^σ is the orbital quasienergy. The normalization condition

$$\langle \phi_k^\sigma\ |\ \phi_k^\sigma\ \rangle=1 \tag{20}$$

is assumed. The solution of the set of TDKS equations (19) can be greatly facilitated by recasting it into a *time-independent* matrix equation by means of the Fourier expansion of the periodic functions $\phi_k^\sigma(\boldsymbol{r},t)$ [19]:

$$\hat{H}_F^\sigma(\boldsymbol{r})\vec{\phi}_k^\sigma=\epsilon_k^\sigma\vec{\phi}_k^\sigma, \tag{21}$$

where $\vec{\phi}_k^\sigma$ is the vector consisting of the Fourier components $\phi_{km}^\sigma(\boldsymbol{r})$ of the function $\phi_k^\sigma(\boldsymbol{r},t)$,

$$\phi_k^\sigma(\boldsymbol{r},t)=\sum_{m=-\infty}^{\infty}\exp(-im\omega t)\phi_{km}^\sigma(\boldsymbol{r}), \tag{22}$$

and $\hat{H}_F^\sigma$ is the Floquet Hamiltonian matrix obtained upon substitution of the expansion (22) into the TDKS (19) [19]. The Floquet Hamiltonian matrix eigenvalue problem (21) is to be solved through the self-consistent procedure until convergence is reached.

In the presence of intense external electromagnetic fields, atoms (molecules) can be ionized (dissociated) by the absorption of multiple photons, and all the bound states become *shifted* and *broadened* resonance states possessing *complex quasienergies* $\varepsilon=\varepsilon_r-i\Gamma/2$. The real parts of the complex quasienergies ε_r provide the ac Stark shifted energy levels, while Γ are equal to the total ionization (dissociation) rates of the corresponding atomic (molecular) states. To determine these complex quasienergy states, the previously developed *non-Hermitian Floquet Hamiltonian formalisms* [18,27], which employ the use of the complex-scaling transformation methods [28], can be extended to TDDFT [19–22]. The use of the complex-scaling transformations $r\rightarrow R(r)$, allows the analytical continuation of the Hermitian Floquet Hamiltonian $\hat{H}_F^\sigma(r)$ [Eq. (21)], into a *non-Hermitian* Floquet Hamiltonian $\hat{H}_F^\sigma(R(r))$, reducing the problem of the determination of the complex-quasienergy eigenvalues ϵ_k^σ and eigenvectors $\vec{\phi}_k^\sigma$ to the solution of a non-Hermitian ei-

genvalue problem. The complex-scaling transformation $R(r)$ can be a uniform complex scaling, $r \rightarrow r\exp(i\alpha)$, where α is a complex-rotation angle; or an exterior complex scaling (see Sec. III). Note that in the spherical coordinates, the complex-scaling transformation is applied only to the radial coordinate r.

The total quasienergy ε can be expressed through the orbital quasienergies, Hartree and exchange-correlation energies, as well as through the expectation values of the exchange-correlation potentials [19–22]:

$$\varepsilon = \sum_{k,\sigma} \epsilon_k^\sigma + \frac{1}{T}\int_0^T dt \Bigg[E_{xc}(t) - J(t) - \sum_\sigma \int d^3 r v_{xc}^\sigma(\mathbf{r},t)\rho^\sigma(\mathbf{r},t) \Bigg]. \tag{23}$$

The analytical continuation in the complex plane of the radial coordinate r corresponding to the complex-scaling transformation preserves that the spin densities remain real quantities for the real values of r [20]. That is why all the contributions to the right-hand side of Eq. (23) are real, except the eigenvalues ϵ_k^σ. Thus the *total* ionization rate can be expressed as a sum of *spin-orbital* ionization rates [20]:

$$\Gamma = \sum_{k,\sigma} \Gamma_k^\sigma, \tag{24}$$

where the spin-orbital rates Γ_k^σ are related to the imaginary parts of the orbital quasienergies as usual,

$$\Gamma_k^\sigma = -2\ \mathrm{Im}\ \epsilon_k^\sigma. \tag{25}$$

In the present TDDFT calculations, we make use of the (spin-polarized) Becke exchange [29] and Lee-Yang-Parr correlation [30] functionals (BLYP exchange correlation). For the self-interaction correction, we extend the Krieger-Li-Iafrate (KLI) procedure [31,32] with the implementation of an explicit self-interaction-correction term [33]. The combination of BLYP exchange-correlation and KLI self-interaction correction (BLYP-KLI/SIC) has proved its accuracy in extensive atomic structure calculations [33,34]. For TDDFT, as a conventional choice, we adopt the adiabatic approximation that employs the same exchange-correlation functionals as in the time-independent theory, but calculates them with the time-dependent spin densities.

When applying a complex-scaling transformation, a delicate task is to perform the analytical continuation of the exchange-correlation potential which depends on the spin densities ρ^σ, to the complex plane. Usually this potential exhibits very complicated functional form that may or may not allow to obtain accurate results with the uniform-complex-scaling technique. The exterior-complex-scaling procedure (Sec. III) allows the overcome of these difficulties.

III. EXTERIOR-COMPLEX-SCALING–GENERALIZED-PSEUDOSPECTRAL METHOD FOR ATOMIC AND MOLECULAR RESONANCES

The exterior-complex-scaling (ECS) transformation was first proposed by Simon [35] for the treatment of molecular resonances in the Born-Oppenheimer approximation. It has been subsequently extended to the study of atomic and molecular resonances, particularly, for potentials which behave nonanalytically (or defined only numerically or piecewise analytically) in the interior region of the coordinates. The principal idea of ECS is to perform the analytical continuation (complex scaling) of the coordinates beyond some distance R_b only. Thus for the one-particle system, the contour $R(r)$ in the complex plane of the coordinate can be defined as follows:

$$R(r) = r, \quad 0 \leqslant r \leqslant R_b,$$

$$R(r) = R_b + (r - R_b)\exp(i\alpha), \quad r > R_b. \tag{26}$$

Here r is assumed to be real valued while $R(r)$ becomes complex valued beyond the radius R_b. For many-body systems, the same transformation is performed for each interparticle coordinate. A number of applications of the exterior-complex-scaling procedure has been developed in the time-independent calculations of atomic and molecular resonances [36–40], cross sections in electron-atom collisions [41], as well as in time-dependent calculations [42].

In our recent paper [23], we introduced an implementation of the exterior-scaling method by means of the generalized-pseudospectral (GPS) technique [43–45], providing a simple yet highly accurate and efficient procedure. The *uniform* complex scaling within this GPS method was successfully applied for atomic and molecular resonance calculations (see, e.g., Refs. [43,44,46–49]). According to this CSGPS approach, the complex-rotated coordinate is discretized on a set of collocation grid points, the potential matrix elements being diagonal and equal to the values of the potential at the grid points. The kinetic-energy matrix elements have simple explicit analytical expressions. As discussed elsewhere [43,45], this uniform CSGPS procedure is found to be highly accurate and computationally more efficient than the traditional basis-set expansion method. For the *exterior* scaling, the whole range of the coordinate is split into two domains, the pseudospectral discretization being performed separately in each domain. The complex scaling is applied in the exterior domain only. The boundary conditions at the boundary point R_b can be incorporated in the discretized Hamiltonian, modifying the matrix elements. The new matrix elements also have simple explicit expressions, and the calculation of the Hamiltonian matrix in the generalized-pseudospectral method with the exterior complex scaling is as simple as with the uniform complex scaling. The ECSGPS method for atomic and molecular resonances has proven its accuracy and efficiency in treatment of multiphoton quasienergy resonances [23] (within the non-Hermitian Floquet Hamiltonian formalism [18,27]). The details of the method have been presented elsewhere [23]. In

this section, we review the basic equations that are required for the computational algorithm.

The complex-scaling–generalized-pseudospectral (CSGPS) method for discretization and solution of eigenvalue problems [43,45] employs orthogonal polynomials (such as Legendre or Chebychev polynomials) and allows for *nonuniform* grid spacing. For problems involving singularity and/or long-range potentials (such as the Coulomb potential), the CSGPS method with appropriate coordinate mapping [43,45] is a natural and effective approach. Applying the complex scaling allows for successful treatment of bound as well as resonance states.

The exterior complex scaling assumes that only the exterior part of the radial coordinate semiaxis is complex rotated. That means the total semiaxis $[0,\infty]$ is divided in two domains $[0,R_b]$ and $[R_b,\infty]$ with the pseudospectral discretization applied separately in each domain. In our discretization, we employ the Legendre polynomials that are orthogonal on the interval $[-1,1]$. The appropriate transformations are used to map the domains on the radial coordinate semiaxis to this interval.

For the exterior domain, one can use the following nonlinear mapping transformation $r_{ex}(x)$ [23]:

$$r_{ex}=R_b+R_{ex}\frac{1+x}{1-x}\exp(i\alpha), \tag{27}$$

α being the complex-rotation angle. Unlike our previous paper [23], in the interior domain we also will apply the nonlinear map $r_{in}(x)$,

$$r_{in}=R_{in}\frac{1+x}{1-x+2R_{in}/R_b}. \tag{28}$$

Using the nonlinear map (28) in the interior domain can provide a better description of the Coulomb singularity and long-range tail for inner-shell orbitals of a multielectron atom. The boundary point R_b, as well as R_{in}, R_{ex}, and α are the parameters of the transformations. For mathematically exact implementation of the ECS and mapping transformations, the resulting eigenvalues do not sensitively depend on these parameters and remain stationary for a range of the complex-rotation angle α. For any approximate (numerical) method, such dependence may appear. However, ECSGPS method is highly accurate, and no dependence on the parameters has been detected in the vicinity of the values used in the calculations (see below in Sec. IV).

Let $\{x_j^{in}\}$, $j=0,\ldots,N_{in}$ and $\{x_j^{ex}\}$, $j=0,\ldots,N_{ex}$ be the sets of the grid points in the interior and exterior domains, respectively. The subscript j values 0 and N_{in}, N_{ex} correspond to the end points of the interval $[-1,1]$:

$$x_0^{in}=x_0^{ex}=-1,$$

$$x_{N_{in}}^{in}=x_{N_{ex}}^{ex}=1. \tag{29}$$

Now consider the eigenvalue problem for the radial Schrödinger equation defined on the semi-infinite axis $[0,\infty]$ with the Dirichlet boundary conditions:

$$\hat{H}(r)\psi(r)=E\psi(r), \quad \psi(0)=\psi(\infty)=0, \tag{30}$$

where

$$\hat{H}(r)=-\frac{1}{2}\frac{d^2}{dr^2}+V(r). \tag{31}$$

One can define the coefficients A_j^{in} and A_j^{ex} related to the wave-function values at the grid points in the interior and exterior domains, respectively [23],

$$A_j^{in}=\left[\frac{dr_{in}}{dx}(x_j^{in})\right]^{1/2}\psi(r_{in}(x_j^{in}))[P_{N_{in}}(x_j^{in})]^{-1},$$

$$A_j^{ex}=\left[\frac{dr_{ex}}{dx}(x_j^{ex})\right]^{1/2}\psi(r_{ex}(x_j^{ex}))[P_{N_{ex}}(x_j^{ex})]^{-1}, \tag{32}$$

$P_N(x)$ being the Legendre polynomials. Then the eigenvalue problem for the wave function $\psi(r)$ is reduced to the matrix eigenvalue problem for the coefficients A_j^{in} and A_j^{ex}:

$$\sum_{j=1}^{N_{in}-1}\left[H_{j'j}^{in}-\frac{1}{\nu}H_{j',N_{in}}^{in}D_{N_{in},j}^{in}\right]A_j^{in}+(-1)^{N_{ex}}\frac{\mu}{\nu}H_{j',N_{in}}^{in}\sum_{j=1}^{N_{ex}-1}D_{0,j}^{ex}A_j^{ex}=EA_{j'}^{in}, \quad j'=1,\ldots,N_{in}-1,$$

$$\sum_{j=1}^{N_{ex}-1}\left[H_{j'j}^{ex}+\frac{1}{\nu}H_{j',0}^{ex}D_{0,j}^{ex}\right]A_j^{ex}-(-1)^{N_{ex}}\frac{1}{\mu\nu}H_{j',0}^{ex}\sum_{j=1}^{N_{in}-1}D_{N_{in},j}^{in}A_j^{in}=EA_{j'}^{ex}, \quad j'=1,\ldots,N_{ex}-1. \tag{33}$$

Here the constants μ and ν are defined as follows:

$$\mu=\left[\frac{dr_{in}}{dx}(1)\right]^{1/2}\left[\frac{dr_{ex}}{dx}(-1)\right]^{-1/2},$$

$$\nu=\frac{1}{4}\left\{N_{in}(N_{in}+1)\left[\frac{dr_{in}}{dx}(1)\right]^{-1}+N_{ex}(N_{ex}+1)\left[\frac{dr_{ex}}{dx}(-1)\right]^{-1}\right\}, \tag{34}$$

and $H_{j'j}^{in}$ and $H_{j'j}^{ex}$ are the matrix elements of the Hamiltonian as defined by the GPS method [43,45]:

$$H_{j'j}^{in}=T_{j'j}^{in}+\delta_{j'j}V(r_{in}(x_j^{in})),$$

$$H_{j'j}^{ex}=T_{j'j}^{ex}+\delta_{j'j}V(r_{ex}(x_j^{ex})). \tag{35}$$

The kinetic-energy matrix elements $T^{in}_{j'j}$, $T^{ex}_{j'j}$ and the first derivative matrix elements $D^{in}_{j'j}$, $D^{ex}_{j'j}$ are calculated as follows:

$$T^{in}_{j'j}=\left[\frac{dr_{in}}{dx}(x^{in}_{j'})\right]^{-1/2} d^{(2),in}_{j'j}\left[\frac{dr_{in}}{dx}(x^{in}_{j})\right]^{-1/2},$$

$$T^{ex}_{j'j}=\left[\frac{dr_{ex}}{dx}(x^{ex}_{j'})\right]^{-1/2} d^{(2),ex}_{j'j}\left[\frac{dr_{ex}}{dx}(x^{ex}_{j})\right]^{-1/2}, \quad (36)$$

$$D^{in}_{j'j}=\left[\frac{dr_{in}}{dx}(x^{in}_{j'})\right]^{-1/2} d^{(1),in}_{j'j}\left[\frac{dr_{in}}{dx}(x^{in}_{j})\right]^{-1/2},$$

$$D^{ex}_{j'j}=\left[\frac{dr_{ex}}{dx}(x^{ex}_{j'})\right]^{-1/2} d^{(1),ex}_{j'j}\left[\frac{dr_{ex}}{dx}(x^{ex}_{j})\right]^{-1/2}. \quad (37)$$

Finally, the fundamental matrix elements $d^{(1),in}_{j'j}$, $d^{(1),ex}_{j'j}$ and $d^{(2),ex}_{j'j}$, $d^{(2),ex}_{j'j}$ depend on the pseudospectral grid point sets $\{x^{in}_j\}$ and $\{x^{ex}_j\}$ only, and have the following expressions for the subscript range appearing in Eq. (33):

$$d^{(1),in}_{j'j}=\frac{1}{x^{in}_{j'}-x^{in}_{j}} \quad (j'\neq j), \quad d^{(1),in}_{jj}=0,$$

$$d^{(1),ex}_{j'j}=\frac{1}{x^{ex}_{j'}-x^{ex}_{j}} \quad (j'\neq j), \quad d^{(1),ex}_{jj}=0, \quad (38)$$

$$d^{(2),in}_{j'j}=-\frac{2}{(x^{in}_{j'}-x^{in}_{j})^2} \quad (j'\neq j),$$

$$d^{(2),in}_{jj}=-\frac{N(N+1)}{3(1-[x^{in}_{j}]^2)},$$

$$d^{(2),ex}_{j'j}=-\frac{2}{(x^{ex}_{j'}-x^{ex}_{j})^2} \quad (j'\neq j),$$

$$d^{(2),ex}_{jj}=-\frac{N(N+1)}{3(1-[x^{ex}_{j}]^2)}. \quad (39)$$

Note that the coefficients $A^{in}_{N_{in}}$ and A^{ex}_0, corresponding to the boundary point R_b, do not appear in the matrix eigenvalue problem (33). The boundary conditions at the point R_b are incorporated into the Hamiltonian matrix modifying its matrix elements in the interior and exterior domains as well as adding coupling matrix elements between the two domains. The total matrix of the eigenvalue problem (33) has the dimensions $(N_{in}+N_{ex}-2)$ by $(N_{in}+N_{ex}-2)$. The diagonalization of this matrix yields the eigenvalues and the eigenvectors $\{A^{in}_j\}$ and $\{A^{ex}_j\}$ inside the interior and exterior domains. Then the coefficients $A^{in}_{N_{in}}$ and A^{ex}_0, corresponding to the boundary point R_b (and the wave function at the boundary point R_b), can be calculated through the other coefficients A^{in}_j and A^{ex}_j:

$$A^{in}_{N_{in}}=-\frac{1}{\nu}\left[\sum_{j=1}^{N_{in}-1} D^{in}_{N_{in},j}A^{in}_j+(-1)^{N_{ex}-1}\mu\sum_{j=1}^{N_{ex}-1} D^{ex}_{0,j}A^{ex}_j\right], \quad (40)$$

$$A^{ex}_0=\frac{1}{\nu}\left[\sum_{j=1}^{N_{ex}-1} D^{ex}_{0,j}A^{ex}_j+(-1)^{N_{ex}-1}\frac{1}{\mu}\sum_{j=1}^{N_{in}-1} D^{in}_{N_{in},j}A^{in}_j\right]. \quad (41)$$

The application of ECSGPS method to calculation of atomic or molecular resonances in TDDFT is similar to that of the uniform-CSGPS method [43,46,47] in our previous work [19–21], except the radial distance r is partitioned into the interior and exterior regions [Eq. (26)]. The optimal distance R_b to partition the two regions can be chosen in such a way that the most complicated but short-range interaction (such as exchange-correlation potential) is included in the interior region, while the exterior region includes only the long-range part of the interaction (such as Coulomb and centrifugal potentials). For sufficiently large R_b, the calculation of the partial rates and angular distributions can be basically accomplished within the interior region [23], resulting in a significant simplification of the overall procedure.

IV. CALCULATIONS OF PARTIAL RATES AND ELECTRON ANGULAR DISTRIBUTIONS FOR MULTIPHOTON ABOVE-THRESHOLD DETACHMENT OF Li^-

In this section, we apply the ECSGPS method to the self-consistent solution of the non-Hermitian Floquet Hamiltonian associated with multiphoton detachment of Li^- in monochromatic linearly polarized laser field.

With no external field, the electron affinity of Li as calculated by DFT with BLYP exchange correlation and KLI self-interaction correction is 0.022 94 a.u. which is in good agreement with the experimental value of 0.022 71 a.u. (see Ref. [50] and references therein). To determine the electron affinity, we used the energy of the highest occupied spin orbital. In the *exact* Kohn-Sham theory, the energy of the highest occupied spin orbital is equal to the negative ionization potential (electron affinity) of the system (ionization theorem [51]). In the optimized effective potential method [52–54] and its simplified version—KLI procedure [31,32]—the ionization theorem [51] is approximately satisfied with a good accuracy when E_{xc} includes self-interaction corrections [33,55], and it is the case for the BLYP-KLI/SIC functional. Note that an accurate description of the highest occupied spin orbital is extremely important in the ionization or detachment problems.

The procedure for the calculation of electron energy and angular distributions within the Floquet formalism has been described elsewhere [47]. Here we outline the basic formulas for the description of multiphoton detachment of Li^-. The expression for the electron angular distributions after absorption of n linearly polarized photons can be written as [47]

$$\frac{d\Gamma_n}{d\Omega}=(2\pi)^{-2}k_n|A_n|^2. \quad (42)$$

Here,

$$k_n = \sqrt{2(\mathrm{Re}\,\varepsilon - (2\omega)^{-2}F^2 + n\omega)} \tag{43}$$

is the electron drift momentum, and the n-photon detachment amplitude A_n is defined as follows [47,56]:

$$A_n = (2\pi)^{-1}\int_{-\pi}^{\pi} d\tau \exp[in\tau - i(2\omega)^{-3}F^2\sin(2\tau) + ik_n(\hat{\boldsymbol{r}}\cdot\boldsymbol{F})\omega^{-2}\cos\tau]\int d^3r' \exp[-ik_n(\hat{\boldsymbol{r}}\cdot\boldsymbol{r}') + i(\boldsymbol{r}'\cdot\boldsymbol{F})\omega^{-1}\sin\tau]W(\boldsymbol{r}',\tau/\omega)\ \ \phi(\boldsymbol{r}',\tau/\omega), \tag{44}$$

$\boldsymbol{F}$ and ω being the laser field strength and frequency, respectively. Equation (44) is an *exact* result of the Green's-function approach to the solution of the one-electron time-dependent Schrödinger equation with the external field being monochromatic and described in the dipole approximation. The form of the amplitude (44) assumes that the *length* gauge is used to solve for the *exact* wave function $\phi(\boldsymbol{r},t)$. In the present consideration, we apply this single-electron theory to the highest occupied $(2s)$ spin orbital of Li^- which is responsible for the detachment process in the laser frequency and intensity range under consideration. Thus the time-dependent potential $W(\boldsymbol{r},t)$ in Eq. (44) is a self-consistent potential including the interaction with the nucleus, the Hartree and exchange-correlation potentials:

$$W(\boldsymbol{r},t) = u(\boldsymbol{r}) + v_H(\boldsymbol{r},t) + v_{xc}(\boldsymbol{r},t), \tag{45}$$

and $\phi(\boldsymbol{r},t)$ is the wave function of the highest occupied $(2s)$ spin orbital of Li^-. The expression (44) is suitable for practical computations since the integration over the angles in the spatial integral can be performed analytically, and the integral over the τ variable can be computed effectively using the fast-Fourier-transform routines. The quantity $d\Gamma_n/d\Omega$ represents the number of electrons per unit time detached with absorption of n photons and emitted within the unit solid angle under direction of the unit vector $\hat{\boldsymbol{r}}$. The integration of the angular distributions (42) with respect to the angles specifying the direction $\hat{\boldsymbol{r}}$ gives the partial rates Γ_n:

$$\Gamma_n = \int d\Omega \frac{d\Gamma_n}{d\Omega}. \tag{46}$$

The sum of all partial rates with $n \geqslant n_{min}$, where n_{min} is the minimum number of photons required for detachment, is equal to the total rate Γ:

$$\Gamma = \sum_{n=n_{min}}^{\infty} \Gamma_n. \tag{47}$$

One can expand $d\Gamma_n/d\Omega$ as a function of the angle θ between the detection $\hat{\boldsymbol{r}}$ and field $\boldsymbol{F}$ directions on the basis of the Legendre polynomials. Due to parity restrictions, only even Legendre polynomials are present in the expansion

$$\frac{d\Gamma_n}{d\Omega} = \frac{\Gamma_n}{4\pi}\left(1 + \sum_{l=1}^{\infty} \beta_{2l}P_{2l}(\cos\theta)\right). \tag{48}$$

The coefficients β_{2l} are the anisotropy parameters since they determine the deviation of the electron angular distribution from the isotropic one. When analyzing the behavior of the coefficients β_{2l} for weak and medium-strong external fields, a comparison with the results of the lowest-order perturbation theory (LOPT) is valuable. For the one-photon detachment, the prediction of the perturbation theory is $\beta_2 = 2$, $\beta_{2l} = 0$ $(l > 1)$. The situation is more complicated if the number of absorbed photons $n = 2$. According to LOPT, the emitted electrons in this case may possess the angular momentum 0 or 2. For the emitted electron in the pure d state, one has $\beta_2 = 10/7$, $\beta_4 = 18/7$, and $\beta_{2l} = 0$ $(l > 2)$; whereas for the pure s state the distribution is isotropic, all $\beta_{2l} = 0$. In reality, however, s and d waves are mixed in the wave function of the emitted electron. According to LOPT, the dependence of the detachment amplitude on the detection angle θ between the vectors $\boldsymbol{F}$ and $\hat{\boldsymbol{r}}$ reduces to a linear combination of s- and d-partial waves,

$$\delta\ \sqrt{\frac{1}{2}}P_0(\cos\theta) + \sqrt{\frac{5}{2}}P_2(\cos\theta). \tag{49}$$

The factors $\sqrt{1/2}$ and $\sqrt{5/2}$ are added as normalization coefficients for the Legendre polynomials. The mixing coefficient δ is a complex number; in general, it depends not only on the angular algebra, but also on the radial wave functions. Squaring the absolute value of the amplitude written above and expanding it over the even-order Legendre polynomials, one obtains for the coefficients β_2 and β_4,

$$\beta_2 = \frac{10 + 14\sqrt{5}\,\mathrm{Re}\,\delta}{7(1 + |\delta|^2)},$$

$$\beta_4 = \frac{18}{7(1 + |\delta|^2)}, \tag{50}$$

other coefficients being zero within LOPT. Given the mixing coefficient δ, one can calculate the anisotropy parameters β_2 and β_4. For example, if one puts $\delta = 0$ (pure d wave in the final state), the results 10/7 and 18/7 mentioned above are obtained. On the other hand, if we take the β_2 and β_4 coefficients from our calculations, we can find the real part and the absolute value of the mixing coefficient δ:

$$\mathrm{Re}\,\delta = \frac{9\beta_2/\beta_4 - 5}{7\sqrt{5}},$$

$$|\delta| = \sqrt{\frac{18}{7\beta_4} - 1}. \tag{51}$$

The imaginary part $\mathrm{Im}\,\delta$ of the mixing coefficient can be calculated as

$$\mathrm{Im}\,\delta = \pm\sqrt{|\delta|^2 - (\mathrm{Re}\,\delta)^2}. \tag{52}$$

The sign of Im δ cannot be determined from this analysis since the angular distributions do not depend on this sign. The coefficient δ calculated in this way is intensity dependent. In the limit of the weak external field, this result should converge to the intensity-independent value that can be determined within LOPT.

A similar analysis can be performed for the case of three-photon detachment. According to LOPT, the detached electron can be either in p or in f state, with the detachment amplitude depending on the angle θ as

$$\delta \quad \sqrt{\frac{3}{2}}P_1(\cos\theta)+\sqrt{\frac{7}{2}}P_3(\cos\theta). \tag{53}$$

The expression of the anisotropy parameters β_{2l} through the mixing coefficient δ now appears as follows:

$$\beta_2=2+\frac{18\sqrt{3/7}\,\mathrm{Re}\,\delta-2}{3(1+|\delta|^2)},$$

$$\beta_4=\frac{264\,\mathrm{Re}\,\delta+18}{11(1+|\delta|^2)},$$

$$\beta_6=\frac{100}{33(1+|\delta|^2)}, \tag{54}$$

other coefficients β_{2l} being zero within LOPT. For the emitted electron in the pure p state, one has $\beta_2=2$, $\beta_4=\beta_6=0$; whereas in the pure f state the values of the anisotropy parameters are as follows: $\beta_2=4/3$, $\beta_4=18/11$, and $\beta_6=100/33$. Using any two of the Eqs. (54), one can invert them and obtain expressions of the mixing parameter δ through the coefficients β_{2l}. For example, the following relations hold:

$$\mathrm{Re}\,\delta=\sqrt{21}\left[\frac{25\beta_4}{198\beta_6}-\frac{3}{44}\right],$$

$$|\delta|=\sqrt{\frac{100}{33\beta_6}-1}. \tag{55}$$

Again, the imaginary part Im δ of the mixing coefficient can be calculated according to Eq. (52), and its sign cannot be determined from the angular distributions. The intensity-dependent mixing parameter δ calculated by Eq. (55) in the weak-field limit should converge to the intensity-independent value provided by LOPT. The remaining third equation of the set (54) can be used to check if the LOPT picture, assumed by Eq. (53), is really applicable, and to check the consistency of the calculations in this sense. Certainly, for intense external fields the mixing coefficient δ can be used only for approximate analysis of the angular distributions, the accurate analysis being provided by the anisotropy parameters β_{2l}.

We have performed the calculations of the total and partial (above-threshold) multiphoton detachment rates as well as the angular distributions of the emitted electrons. In practical computations, the parameters of the ECSGPS procedure were chosen as follows to achieve convergence:

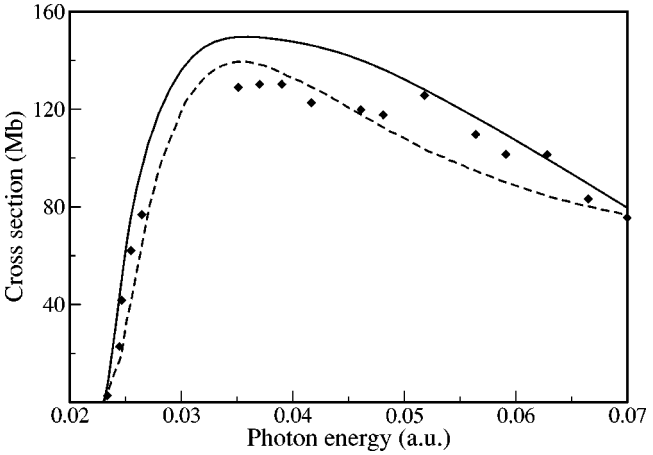

FIG. 1. Cross section of one-photon detachment of Li^-. The full curve is for the present calculation; the dashed curve is for the multichannel R-matrix calculation [58]; diamonds are for experiment [59].

$$R_b=40 \text{ a.u.},$$

$$R_{in}=5 \text{ a.u.},$$

$$R_{ex}=100 \text{ a.u.},$$

$$\alpha=0.6 \text{ rad}. \tag{56}$$

Up to 100 radial grid points were used in each interior and exterior domain. The selected eigenvalue and eigenvector of the non-Hermitian Floquet Hamiltonian matrix can be obtained efficiently by means of the implicitly restarted Arnoldi algorithm [57] with spectral transformation. The interior domain appears large enough to get the integral (44) fully converged within it. That means we do not need to perform the integration in the complex-rotated exterior domain using the *backrotation* procedure as in the uniform-complex-scaling case [46]. This simplifies considerably the calculation of partial rates and angular distributions.

A. One-photon detachment of Li^-

First, we have performed the calculations of the weak-field one-photon detachment cross section. The results are presented in Fig. 1. For comparison, also shown are the results of multichannel R-matrix calculation [58] and experimental data by Kaiser *et al.* [59]. Surprisingly, this early nonlaser experiment remains the only one where the data were obtained for the wide photon energy range between the first and second thresholds. The newer experiments seem to concentrate on narrow energy intervals in the vicinity of higher thresholds. The present single-determinant calculations cannot reproduce the cusp structure in the vicinity of the second $(2p)$ threshold. With this exception, our results are in fair agreement with the more sophisticated multichannel calculations [58] and with the experiment [59]. Our calculated cross section reaches the maximum of 149.6 Mb at the photon

TABLE I. Partial and total rates for the multiphoton above-threshold detachment of Li^-. The numbers in brackets indicate the powers of 10.

Laser field frequency (a.u.)	Partial rates (a.u.) Number of photons absorbed 2	3	4	Total rates (a.u.)	Re ϵ (a.u.)
		Laser field intensity (1×10^9 W/cm^2)			
0.012	3.90[−8]	6.70[−10]		3.97[−8]	−2.296[−2]
0.014	4.81[−8]	2.77[−10]		4.84[−8]	−2.296[−2]
0.016	4.33[−8]	1.06[−10]		4.34[−8]	−2.297[−2]
0.018	3.08[−8]	3.63[−11]		3.09[−8]	−2.297[−2]
0.020	1.90[−8]	1.21[−11]		1.90[−8]	−2.298[−2]
		Laser field intensity (1×10^{10} W/cm^2)			
0.012	2.44[−6]	7.97[−7]	4.39[−8]	3.28[−6]	−2.341[−2]
0.014	4.08[−6]	2.14[−7]	6.84[−9]	4.30[−6]	−2.322[−2]
0.016	3.82[−6]	9.21[−8]	1.40[−9]	3.91[−6]	−2.321[−2]
0.018	2.87[−6]	3.11[−8]	4.07[−10]	2.90[−6]	−2.323[−2]
0.020	1.86[−6]	1.00[−8]	1.67[−10]	1.87[−6]	−2.330[−2]
		[a]Laser field intensity (1×10^{11} W/cm^2)			
0.012		7.09[−5]	2.06[−5]	9.96[−5]	−2.601[−2]
0.014		3.80[−5]	1.49[−5]	5.60[−5]	−2.659[−2]
0.016	8.02[−5]	4.59[−5]	8.78[−6]	1.36[−4]	−2.768[−2]
0.018	1.41[−4]	2.63[−5]	3.47[−6]	1.71[−4]	−2.690[−2]
0.020	1.40[−4]	1.13[−5]	1.33[−6]	1.53[−4]	−2.649[−2]

[a]At the intensity 1×10^{11} W/cm^2, the two-photon detachment channel is closed for the frequencies 0.012 and 0.014 a.u. due to ac Stark shift of the quasienergy level and ponderomotive shift of the continuum.

energy 0.036 a.u.; the corresponding results of Ref. [58] are 139.9 Mb and 0.035 a.u., respectively.

B. Two-photon dominant, above-threshold detachment of Li^-

The main part of the present calculations was performed for the two-photon dominant, above-threshold detachment of Li^-. We have selected a set of photon energies (0.012, 0.014, 0.016, 0.018, and 0.020 a.u.) corresponding to the two-photon dominant detachment. For this range of photon energies, the second threshold region of Li^- is not approached even for four-photon above-threshold detachment, so the limitations of the current single-configuration calculations do not affect the results. The calculations have been performed for the following values of the laser field intensities 1×10^9, 1×10^{10}, and 1×10^{11} W/cm^2. We have computed the

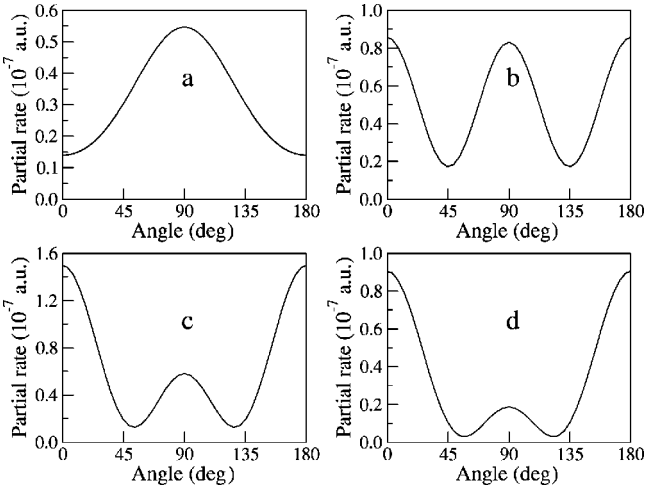

FIG. 2. Angular distributions for two-photon detachment of Li^-. The laser field intensity is 1×10^9 W/cm^2. The laser field frequency is (a) 0.012 a.u., (b) 0.014 a.u., (c) 0.016 a.u., and (d) 0.020 a.u.

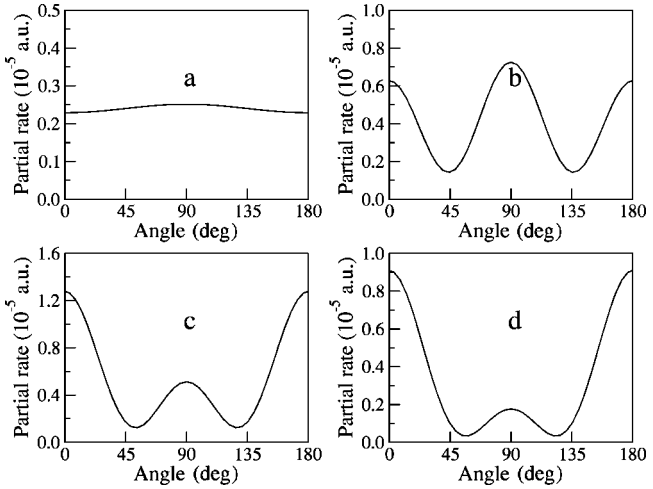

FIG. 3. Angular distributions for two-photon detachment of Li^-. The laser field intensity is 1×10^{10} W/cm^2. The laser field frequency is (a) 0.012 a.u., (b) 0.014 a.u., (c) 0.016 a.u., and (d) 0.020 a.u.

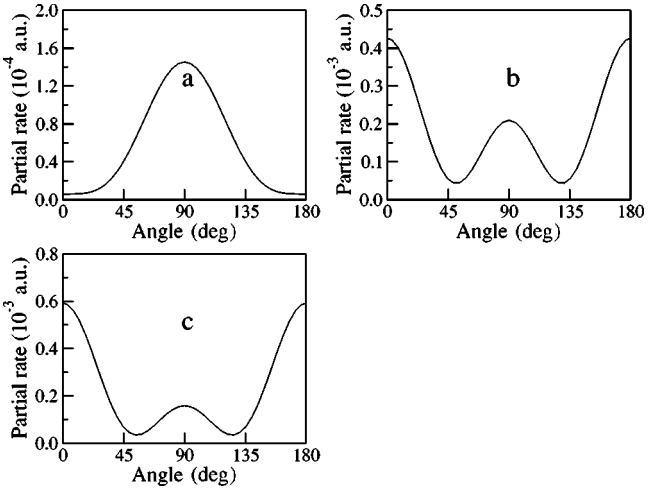

FIG. 4. Angular distributions for two-photon detachment of Li^-. The laser field intensity is 1×10^{11} W/cm^2. The laser field frequency is (a) 0.016 a.u., (b) 0.018 a.u., and (c) 0.020 a.u.

partial rates for the dominant and above-threshold channels (electron energy distributions) as well as the angular distributions of the outgoing electrons.

The partial and total rates along with the real parts of the $2s$ orbital quasienergy are presented in Table I. Generally, for all intensities used in the calculations, the total detachment rates reach the maximum values in the middle of the frequency range, decreasing towards the two-photon threshold on the side of low frequencies and towards the higher frequencies. With increasing intensity, the contribution of the above-threshold channels to the total rate becomes more significant. For the photon energy 0.012 a.u., which lies close to the two-photon threshold, is in part due to the ac Stark shift of the quasienergy level and ponderomotive shift of the continuum. As the intensity increases to 1×10^{10} W/cm^2, the level is shifted even more to the threshold, the two-photon channel begins closing, and the contribution of the three-photon detachment becomes very important (about 33% of the dominant two-photon channel compared to 1.7% at the intensity 1×10^{9} W/cm^2). When the intensity increases to 1×10^{11} W/cm^2, the two-photon detachment channel is closed not only at the frequency 0.012 a.u., but also at 0.014 a.u.

The influence of the threshold causes dramatic changes in the electron angular distributions of the two-photon detachment. The distributions are presented in Figs. 2–4 for the intensities 1×10^{9}, 1×10^{10}, and 1×10^{11} W/cm^2, respectively. The angular distribution pattern shown in Fig. 2 resembles closely that found in the recent experiment on multiphoton detachment of H^- [60]. This is not surprising since both H^- and Li^- represent a negative ion with a short-range interaction between the loosely bound electron and the core. Such atomic systems exhibit similar behavior under the influence of the external electromagnetic fields. Our previous

TABLE II. Anisotropy parameters β_{2l} and the mixing coefficient δ for the two-photon detachment of Li^-. The numbers in brackets indicate the powers of 10.

	Laser field frequency (a.u.)				
	0.012	0.014	0.016	0.018	0.020
			Laser field intensity (1×10^{9} W/cm^2)		
β_2	−7.33[−1]	−4.98[−1]	6.64[−1]	1.28	1.63
β_4	9.14[−2]	1.28	1.80	2.01	2.14
β_6	−1.81[−5]	−1.12[−3]	−1.22[−3]	−1.38[−3]	−4.64[−3]
β_8	2.37[−8]	1.39[−7]	−1.86[−6]	−6.01[−6]	−1.45[−5]
$\lvert\delta\rvert$	5.21	1.01	6.56[−1]	5.29[−1]	4.50[−1]
Re δ	−4.93	−5.43[−1]	−1.07[−1]	4.79[−2]	1.20[−1]
			Laser field intensity (1×10^{10} W/cm^2)		
β_2	−6.14[−2]	−6.57[−1]	5.97[−1]	1.26	1.65
β_4	4.98[−4]	1.20	1.73	1.99	2.14
β_6	6.81[−8]	−4.76[−3]	1.97[−2]	5.69[−2]	9.04[−2]
β_8	3.13[−7]	2.11[−4]	3.68[−4]	1.09[−3]	3.79[−3]
$\lvert\delta\rvert$	7.19[+1]	1.07	6.99[−1]	5.43[−1]	4.47[−1]
Re δ	−7.13[+1]	−6.35[−1]	−1.21[−1]	4.52[−2]	1.24[−1]
			[a]Laser field intensity (1×10^{11} W/cm^2)		
β_2			−1.33	3.13[−1]	1.18
β_4			4.01[−1]	1.71	1.97
β_6			1.49[−4]	−1.58[−3]	6.66[−2]
β_8			5.04[−6]	8.59[−4]	−7.90[−3]
$\lvert\delta\rvert$			2.33	7.10[−1]	5.50[−1]
Re δ			−2.22	−2.14[−1]	2.41[−2]

[a]At the intensity 1×10^{11} W/cm^2, the two-photon detachment channel is closed for the frequencies 0.012 and 0.014 a.u. due to ac Stark shift of the quasienergy level and ponderomotive shift of the continuum.

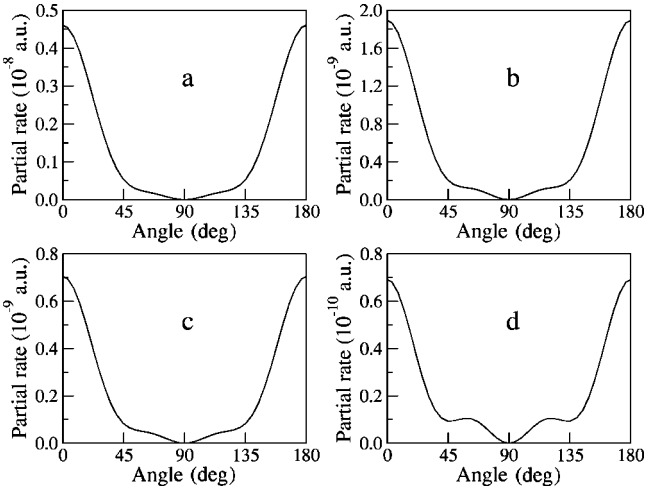

FIG. 5. Angular distributions for three-photon above-threshold detachment of Li^-. The laser field intensity is 1×10^9 W/cm^2. The laser field frequency is (a) 0.012 a.u., (b) 0.014 a.u., (c) 0.016 a.u., and (d) 0.020 a.u.

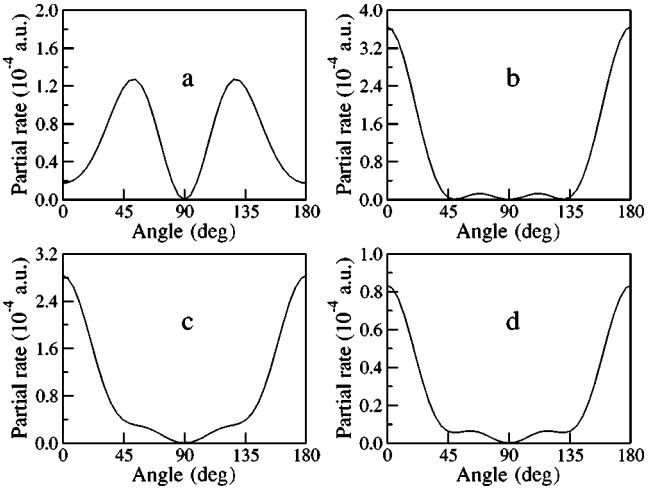

FIG. 7. Angular distributions for three-photon above-threshold detachment of Li^-. The laser field intensity is 1×10^{11} W/cm^2. The laser field frequency is (a) 0.012 a.u., (b) 0.014 a.u., (c) 0.016 a.u., and (d) 0.020 a.u.

model-potential studies of above-threshold multiphoton detachment of H^- [23,47] revealed the same features of the angular distributions and were in good agreement with the experiments at Los Alamos [61] and Denmark [62]. The angular distributions show the interference of *s* and *d* waves in the detachment amplitude. For sufficiently high frequencies (0.016, 0.018, and 0.020 a.u. in our calculations), the *d* wave dominates the amplitude, and the angular distributions show the pattern as in Fig. 2 (c) or in Fig. 2 (d). For smaller frequencies (0.014 and 0.012 a.u.), the quasienergy level is brought closer to the threshold and the relative weight of the *s* wave increases, in accordance with the Wigner threshold law [63]. One can see it also in Table II where we present the anisotropy parameters β_{2l} and the mixing coefficient δ. For smaller frequencies, the anisotropy parameters become smaller and the mixing coefficient increases. Thus at the frequency 0.020 a.u., only 17% of the electrons are detached in the *s* state; 83% being in the *d* state; whereas at the frequency 0.012 a.u., the picture is completely reversed, 96% of *s* electrons and 4% of *d* electrons. For the intensity 1×10^{10} W/cm^2 (Fig. 3), the angular distributions depend on the laser field frequency in a similar manner. At the frequency 0.012 a.u., the distribution becomes nearly isotropic because larger ac Stark and ponderomotive shifts bring the two-photon detachment channel even closer to the threshold. Only 0.02% of electrons are detached in the *d* state at this frequency, others being in the *s* state. For even higher intensity (1×10^{11} W/cm^2), the two-photon detachment channel is closed for the frequencies 0.012 and 0.014 a.u., due to large ac Stark and ponderomotive shift of the quasienergy level. The angular distributions pattern (Fig. 4) resembles that of Fig. 2, but at different photon energies; now detachment at the frequency 0.016 a.u apparently takes place in the vicinity of the two-photon threshold.

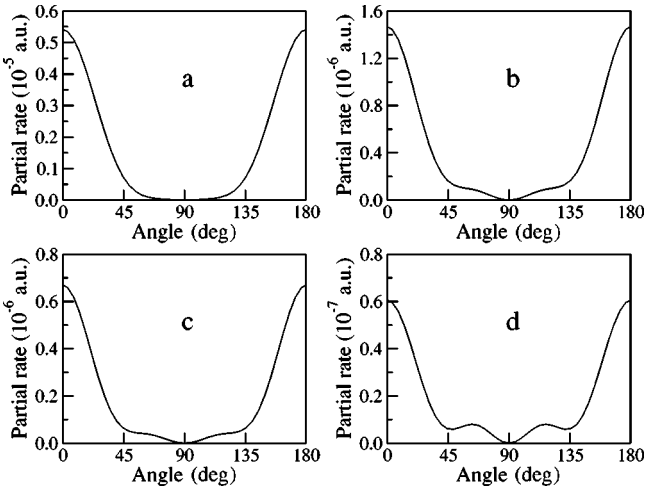

FIG. 6. Angular distributions for three-photon above-threshold detachment of Li^-. The laser field intensity is 1×10^{10} W/cm^2. The laser field frequency is (a) 0.012 a.u., (b) 0.014 a.u., (c) 0.016 a.u., and (d) 0.020 a.u.

For the three-photon above-threshold detachment, the angular distributions do not show dramatic transformations when the frequency is scanned in the range corresponding to the two-photon dominant detachment (Figs. 5 and 6), except for the highest intensity 1×10^{11} W/cm^2 (Fig. 7). Since at the lower intensities 1×10^9 and 1×10^{10} W/cm^2, the threshold for this channel is not approached for the frequency range used in the calculations, only moderate changes can be seen in the angular distributions pattern, with the distribution maximum at 0° (180°), as expected. The anisotropy parameters for the three-photon detachment (Table III) show significant contributions to the detachment amplitude from the angular momenta 1 and 3 (coefficients β_2, β_4, and β_6) as can be expected for weak and medium-strong external fields. The contribution of other coefficients β_{2l} (which are supposed to vanish within LOPT) increases for higher intensities. The absolute value of the mixing coefficient δ generally increases as the photon energy decreases, again in accordance with the Wigner threshold law [63]. For example, at

TABLE III. Anisotropy parameters β_{2l} and the mixing coefficient δ for the three-photon above-threshold detachment of Li^-. The numbers in brackets indicate the powers of 10.

	Laser field frequency (a.u.)				
	0.012	0.014	0.016	0.018	0.020
	Laser field intensity (1×10^9 W/cm^2)				
β_2	2.97	2.78	2.73	2.44	2.00
β_4	2.03	1.96	1.85	1.54	1.24
β_6	8.84[−1]	1.10	1.05	1.14	1.49
β_8	−2.24[−3]	−3.92[−3]	−7.15[−4]	9.28[−4]	3.40[−3]
β_{10}	1.27[−6]	1.91[−6]	−5.48[−7]	−4.97[−6]	−1.73[−5]
$\lvert\delta\rvert$	1.56	1.33	1.38	1.29	1.01
Re δ	1.01	7.17[−1]	7.10[−1]	4.67[−1]	1.70[−1]
	Laser field intensity (1×10^{10} W/cm^2)				
β_2	3.22	2.76	2.82	2.56	2.12
β_4	2.06	1.93	2.10	1.87	1.58
β_6	5.14[−1]	1.12	1.27	1.33	1.52
β_8	−6.48[−3]	2.94[−2]	7.28[−2]	−1.57[−2]	−2.00[−1]
β_{10}	2.88[−5]	3.21[−3]	7.80[−4]	5.76[−4]	1.39[−2]
$\lvert\delta\rvert$	2.21	1.31	1.18	1.13	9.97[−1]
Re δ	2.01	6.87[−1]	6.41[−1]	5.03[−1]	2.89[−1]
	Laser field intensity (1×10^{11} W/cm^2)				
β_2	3.61[−1]	3.32	2.51	2.60	2.62
β_4	−1.67	3.44	1.55	1.90	2.14
β_6	5.88[−1]	1.94	1.11	1.33	1.59
β_8	−2.89[−2]	−8.66[−2]	4.42[−2]	1.49[−2]	8.48[−3]
β_{10}	5.61[−4]	4.38[−4]	−3.08[−2]	2.12[−2]	−1.19[−2]
$\lvert\delta\rvert$	2.04	7.51[−1]	1.32	1.13	9.51[−1]
Re δ	−1.96	7.14[−1]	4.95[−1]	5.17[−1]	4.65[−1]

the intensity 1×10^{10} W/cm^2 the contributions of p and f electrons to the detachment rate constitute, respectively, 83% and 17% for the photon energy 0.012 a.u.; for the photon energy 0.020 a.u., the corresponding contributions are approximately equal to each other, i.e., 50%. The picture changes at the highest intensity (1×10^{11} W/cm^2). The closing of the two-photon detachment channel for the frequencies 0.012 and 0.014 a.u. strongly affects the angular distributions in the three-photon channel. Just below the two-photon threshold, at the photon energy 0.014 a.u., the contribution of f electrons significantly increases (they constitute 64% of the total detachment rate compared to 37% for the same frequency and intensity 1×10^{10} W/cm^2, where the two-photon channel is still open). When the frequency becomes smaller (0.012 a.u.), the vicinity of the three-photon threshold is approached, and the general tendency in the behavior of the angular distributions (based on the Wigner threshold law) is reinstated. The contribution of p electrons reaches 81%, approximately that can be observed for the same frequency and intensity 1×10^{10} W/cm^2. However, the real parts Re δ of the mixing coefficient in these two cases have opposite signs, and the angular distributions look very different [see Figs. 6(a) and 7(a)].

In conclusion, we have presented a ECSGPS numerical procedure within the Floquet formulation of TDDFT for general and accurate calculations of complex-quasienergy resonances associated with multiphoton above-threshold detachment of negative ions. As compared with the uniform-complex-scaling methods, the ECSGPS technique provides more accurate and efficient procedure for the treatment of complicated potentials such as exchange-correlation potentials in TDDFT. Application is made to the study of one-photon detachment and two-photon dominant above-threshold detachment of Li^- ions for a range of laser frequencies and intensities. Dramatic transformations of the angular distributions in the vicinity of the two-photon threshold are observed and analyzed in detail.

ACKNOWLEDGMENTS

This work is partially supported by the U.S. Department of Energy, Office of Science, Office of Basic Energy Science, Division of Chemical Sciences. We acknowledge the support of the Origin2400 supercomputer time by the Kansas Center for Advanced Scientific Computing.

[1] P. Hohenberg and W. Kohn, Phys. Rev. **136**, B864 (1964).
[2] W. Kohn and L.J. Sham, Phys. Rev. **140**, A1113 (1965).
[3] See, e.g., R.G. Parr and W. Yang, *Density-Functional Theory of Atoms and Molecules* (Oxford University Press, Oxford, 1989); R.M. Dreizler and E.K.U. Gross, *Density Functional Theory, An Approach to the Quantum Many-Body Problem* (Springer, Berlin, 1990); *Density Functional Theory*, Vol. 337 of *NATO Advance Study Institute, Series B: Physics*, edited by E.K.U. Gross and R.M. Dreizler (Plenum Press, New York, 1995); N. H. March, *Electron Density Theory of Atoms and Molecules* (Academic Press, San Diego, 1992); *Density Functional Methods in Chemistry*, edited by J.K. Labanowski and J.W. Andzelm (Springer, Berlin, 1991).
[4] A. Zangwill and P. Soven, Phys. Rev. A **21**, 1561 (1980).
[5] B.M. Deb and S.K. Ghosh, J. Chem. Phys. **77**, 342 (1982).
[6] L.J. Bartolotti, Phys. Rev. A **24**, 1661 (1981); **26**, 2243 (1982).
[7] E. Runge and E.K.U. Gross, Phys. Rev. Lett. **52**, 997 (1984); E.K.U. Gross and W. Kohn, *ibid.* **55**, 2850 (1985).
[8] G.D. Mahan and K.R. Subbaswamy, *Local Density Theory of Polarizability* (Plenum Press, New York, 1990).
[9] M. Stener, P. Decleva, and A. Lisini, J. Phys. B **28**, 4973 (1995).
[10] M. Petersilka, U.J. Gossmann, and E.K.U. Gross, Phys. Rev. Lett. **76**, 1212 (1996).
[11] C.A. Ullrich, U.J. Gossmann, and E.K.U. Gross, Phys. Rev. Lett. **74**, 872 (1995).
[12] X.M. Tong and S.I. Chu, Phys. Rev. A **57**, 452 (1998).
[13] C.A. Ullrich and E.K.U. Gross, Comments At. Mol. Phys. **33**, 211 (1997).
[14] X.M. Tong and S.I. Chu, Phys. Rev. A **64**, 013417 (2001).
[15] X. Chu and S.I. Chu, Phys. Rev. A **63**, 023411 (2001).
[16] X. Chu and S.I. Chu, Phys. Rev. A **64**, 063404 (2001).
[17] See, for example, G. Vignale, C. Ullrich, and S. Conti, Phys. Rev. Lett. **79**, 4878 (1997), and references therein.
[18] For reviews on generalized Floquet methods, see S.I. Chu, Adv. At. Mol. Phys. **21**, 197 (1985); Adv. Chem. Phys. **73**, 739 (1989).
[19] D.A. Telnov and S.I. Chu, Chem. Phys. Lett. **264**, 466 (1997).
[20] D.A. Telnov and S.I. Chu, Phys. Rev. A **58**, 4749 (1998).
[21] D.A. Telnov and S.I. Chu, Int. J. Quantum Chem. **69**, 305 (1998).
[22] D.A. Telnov and S.I. Chu, Phys. Rev. A **63**, 012514 (2000).
[23] D.A. Telnov and S.I. Chu, Phys. Rev. A **59**, 2864 (1999).
[24] J.H. Shirley, Phys. Rev. **138**, B979 (1965).
[25] H. Sambe, Phys. Rev. A **7**, 2203 (1973).
[26] A. Görling, Phys. Rev. A **59**, 3359 (1999).
[27] S.I. Chu and W.P. Reinhardt, Phys. Rev. Lett. **39**, 1195 (1977).
[28] E. Balslev and J.M. Combes, Commun. Math. Phys. **22**, 280 (1971); A. Aguilar and J.M. Combes, *ibid.* **22**, 265 (1971).
[29] A.D. Becke, Phys. Rev. A **38**, 3098 (1988); J. Chem. Phys. **96**, 2155 (1992).
[30] C. Lee, W. Yang, and R.G. Parr, Phys. Rev. B **37**, 785 (1988).
[31] J.B. Krieger, Y. Li, and G.J. Iafrate, Phys. Rev. A **45**, 101 (1992).
[32] Y. Li, J.B. Krieger, and G.J. Iafrate, Phys. Rev. A **47**, 165 (1993).
[33] X.M. Tong and S.I. Chu, Phys. Rev. A **55**, 3406 (1997).
[34] X.M. Tong and S.I. Chu, Phys. Rev. A **57**, 855 (1998).
[35] B. Simon, Phys. Lett. **71A**, 211 (1979).
[36] J. Turner and C.W. McCurdy, Chem. Phys. **71**, 127 (1982).
[37] N. Lipkin, N. Moiseyev, and E. Brändas, Phys. Rev. A **40**, 549 (1989).
[38] A. Scrinzi and N. Elander, J. Chem. Phys. **98**, 3866 (1993).
[39] C.A. Nicolaides, H.J. Gotsis, M. Chrysos, and Y. Komninos, Chem. Phys. Lett. **168**, 570 (1990).
[40] N. Rom, N. Moiseyev, and R. Levebvre, J. Chem. Phys. **95**, 3562 (1991).
[41] T.N. Rescigno, M. Baertschy, D. Byrum, and C.W. McCurdy, Phys. Rev. A **55**, 4253 (1997), and references therein.
[42] C.W. McCurdy, C.K. Stroud, and M.K. Wisinski, Phys. Rev. A **43**, 5980 (1991).
[43] J. Wang, S.I. Chu, and C. Laughlin, Phys. Rev. A **50**, 3208 (1994).
[44] X. Chu and S.I. Chu, Phys. Rev. A **63**, 013414 (2001).
[45] G. Yao and S.I. Chu, Chem. Phys. Lett. **204**, 381 (1993).
[46] D.A. Telnov and S.I. Chu, Phys. Rev. A **50**, 4099 (1994).
[47] D.A. Telnov and S.I. Chu, J. Phys. B **29**, 4401 (1996).
[48] D.A. Telnov, J. Wang, and S.I. Chu, Phys. Rev. A **52**, 3988 (1995).
[49] D.A. Telnov and S.I. Chu, Chem. Phys. Lett. **255**, 223 (1996).
[50] G. Haeffler, D. Hanstorp, I. Kiyan, A.E. Klinkmüller, U. Ljungblad, and D.J. Pegg, Phys. Rev. A **53**, 4127 (1996).
[51] J.P. Perdew, R.G. Parr, M. Levy, and J.L. Balduz, Jr., Phys. Rev. Lett. **49**, 1691 (1982).
[52] R.T. Sharp and G.K. Horton, Phys. Rev. **90**, 317 (1953).
[53] J.D. Talman and W.F. Shadwick, Phys. Rev. A **14**, 36 (1976).
[54] M.R. Norman and D.D. Koelling, Phys. Rev. B **30**, 5530 (1984).
[55] J. Chen, J.B. Krieger, Y. Li, and G.J. Iafrate, Phys. Rev. A **54**, 3939 (1996).
[56] D.A. Telnov, J. Phys. B **24**, 2967 (1991).
[57] D.C. Sorensen, SIAM J. Matrix Anal. Appl. **13**, 357 (1992).
[58] C.A. Ramsbottom, K.L. Bell, and K.A. Berrington, J. Phys. B **27**, 2905 (1994).
[59] H.J. Kaiser, E. Heinicke, R. Rackwitz, and D. Feldmann, Z. Phys. **270**, 259 (1974).
[60] R. Reichle, H. Helm, and I.Yu. Kiyan, Phys. Rev. Lett. **87**, 243001 (2001).
[61] X.M. Zhao, M.S. Gulley, H.C. Bryant, C.E.M. Strauss, D.J. Funk, A. Stintz, D.C. Rislove, G.A. Kyrala, W.B. Ingalls, and W.A. Miller, Phys. Rev. Lett. **78**, 1656 (1997).
[62] L. Praestegaard, T. Andersen, and P. Balling, Phys. Rev. A **59**, R3154 (1999).
[63] E.P. Wigner, Phys. Rev. **73**, 1002 (1948).